Original Article

Intravoxel incoherent motion derived liver perfusion/diffusion readouts can be reliable biomarker for the detection of viral hepatitis B induced liver fibrosis

Ting Li[1], Nazmi Che-Nordin[2], Yì Xiáng J. Wáng[2], Peng-Fei Rong[1], Shi-Wen Qiu[2], Sheng-Wang Zhang[1], Pan Zhang[3], Yong-Fang Jiang[4], Olivier Chevallier[5], Feng Zhao[6], Xiao-Yi Xiao[1], Wei Wang[1]

[1]Department of Radiology, The Third Xiangya Hospital, Central South University, Changsha 410013, China; [2]Department of Imaging and Interventional Radiology, Faculty of Medicine, The Chinese University of Hong Kong, New Territories, Hong Kong, China; [3]Department of Infectious Diseases, The Third Xiangya Hospital, Central South University, Changsha 410013, China; [4]Liver Diseases Research Center, The Second Xiangya Hospital, Central South University, Changsha 410013, China; [5]Department of Vascular and Interventional Radiology, François-Mitterrand Teaching Hospital, Université de Bourgogne, Dijon, France; [6]Department of Radiation Oncology, The First Affiliated Hospital, College of Medicine, Zhejiang University, Hangzhou 310000, China

Correspondence to: Dr. Yì Xiáng J. Wáng. Department of Imaging and Interventional Radiology, Faculty of Medicine, The Chinese University of Hong Kong, New Territories, Hong Kong, China. Email: yixiang_wang@cuhk.edu.hk; Dr. Peng-Fei Rong. Department of Radiology, The Third Xiangya Hospital, Central South University, Changsha 410013, China. Email: rongpengfei66@163.com; Dr. Wei Wang. Department of Radiology, The Third Xiangya Hospital, Central South University, Changsha 410013, China. Email: cjr.wangwei@vip.163.com.

Background: Recent two studies reported that intravoxel incoherent motion (IVIM) analysis can separate healthy livers and viral hepatitis B (VHB) induced liver fibrosis. However, in these two studies the starting *b* value for bi-exponential decay analysis was *b* =10 and 15 s/mm^2 respectively. The current study has two primary aims. The first is to further confirm the diagnostic value of IVIM in detecting liver fibrosis. The second is to test whether by sampling very low *b* value densely, then *b* =0 s/mm^2 image could be included to improve IVIM's diagnostic performance.

Methods: This was a prospective study with data acquired at the Third Xiangya Hospital of Central South University, Changsha, China. Healthy volunteers and patients suspected of VHB induced liver fibrosis with liver biopsy performed, as well as hepatocellular carcinoma patients scheduled for surgery, were recruited. All the hepatocellular carcinoma patients had liver fibrosis. After exclusions based on pre-defined criteria for image data quality, for IVIM analysis this study included 20 healthy volunteers; 4 chronic VHB patients with biopsy showing no liver fibrosis; 11 stage-1 liver fibrosis patients, 10 stage-2 liver fibrosis patients, 2 stage-3 liver fibrosis patients, and 5 stage-4 liver fibrosis patients. In the liver fibrosis patients, 1, 19, and 8 cases had inflammation grade-0, grade-1, and grade-2 respectively. The reference IVIM bi-exponential decay curve fitting analysis was segmented fitting performed with *b* =2 s/mm^2 image as the starting point and a threshold-*b* of 60 s/mm^2. This reference fitting method was compared with threshold-*b* of 40 s/mm^2, full fitting, fitting starting from *b* =0, 5, and 10 s/mm^2 respectively. The potential correlation between IVIM readouts and liver function was assessed for the liver fibrosis patients.

Results: Based on the smaller coefficient of variation (CoV) for the volunteer group and the smaller patient/volunteer ratios [= (mean measurement for patient groups)/(mean measurement for healthy volunteers)], the comparison of fitting methods favored the reference approach starting from *b* =2 s/mm^2 with a threshold-*b* of 60 s/mm^2. The IVIM measures of four patients without liver fibrosis resembled those of healthy subjects. PF offered the best diagnostic value for separating healthy livers and fibrotic livers, and a threshold of PF =0.1406 separated all fibrotic livers and healthy livers with an exception of one hepatocellular carcinoma patient (fibrosis grade-2/inflammation grade-2). The correlation between fibrosis grading and inflammation grading was weakly positive; while compared with fibrotic livers with inflammation grade-1, fibrotic livers with inflammation grade-2 showed a trend of higher Dfast. A weak correlation is shown with

lower PF and lower Dfast associated with lower total protein, lower albumin; higher alanine transaminase, higher aspartate transaminase; higher total bilirubin, and higher direct bilirubin.

Conclusions: Segmented-fitting with threshold-*b* =60 s/mm^2 and starting from non-zero very low *b* value outperforms other methods. IVIM has high sensitivity in detecting liver fibrosis, and PF and Dfast have potential correlation with serum liver function biomarkers. IVIM measures and liver fibrosis grading are not in a linear relationship.

Keywords: Intravoxel incoherent motion (IVIM); diffusion; perfusion; liver; fibrosis; inflammation; biomarker

Submitted Jan 03, 2019. Accepted for publication Feb 25, 2019.
doi: 10.21037/qims.2019.02.11
View this article at: http://dx.doi.org/10.21037/qims.2019.02.11

Introduction

Chronic liver disease is a major public health problem worldwide, accounted for approximately 1.3 million deaths worldwide in 2015 (1). Viral hepatitis is the most common blood-borne infection globally. The end result of untreated chronic liver disease is inflammation, loss of liver parenchyma, and healing by fibrosis and regeneration. The response of hepatocytes to inflammation plays a decisive role in the physiopathology of hepatic fibrosis, which involves the recruitment of both pro- and anti-inflammatory cells such as monocytes and macrophages. These processes amplify the response throughout the production of other cytokines and chemokines, which increase the stimulus of hepatic stellate cells by activating proinflammatory cells. Fibrogenic cytokines, such as transforming growth factor beta (TGF-β), activated by macrophages facilitate the trans-differentiation of stellate cells to myofibroblasts, which are the main source of production of extracellular matrix. Originally considered to be irreversible, hepatic fibrosis is now regarded as a dynamic process with the potential for regression. Earlier stage liver fibrosis is more amenable to therapeutic intervention. In the early stages of fibrosis when the cause has been treated (e.g., hepatitis B or C), regression occurs in at least 70% of patients with the right antiviral management (2,3). The regression of liver fibrosis can be complete in early stages, whereas partial and prolonged recovery occurs in late or advanced stages (4). Treatment with combined therapies on underline etiology and fibrosis simultaneously might expedite the regression of liver fibrosis and promote liver regeneration. Early detection of liver fibrosis is important for early institution of treatment and assessing potential for regression and prognosis.

Currently there is no established non-invasive diagnostic method to detect and grade early stage liver fibrosis (5). The reference standard for detection and staging of liver fibrosis remains being biopsy; however, it is invasive and frequently causes pain and discomfort, with risk of bleeding and hospitalization and also not suitable for longitudinal monitoring. The most clinically used imaging technique for evaluation of liver fibrosis is ultrasound elastography, while the investigational technique of MR elastography has undergone many promising clinical trials. The requirement for an external driver is considered a disadvantage for MR elastography. As intravoxel incoherent motion (IVIM) imaging sequence is widely available in clinical MR scanners and there is no need for external device, it represents a convenient alternative to existing techniques for liver fibrosis evaluation. It is well accepted that liver fibrosis is associated with reduced liver perfusion (6-9), and progressive loss of endothelial fenestration and deposition of collagen in the space of Disse. These processes reduce the rate of blood flow and prolong its transit time. Recently there has been a great interest of using IVIM technique to study diffused liver diseases such as liver fibrosis (10).

Recently we published two small cohort studies (11,12), our results suggested that liver IVIM analysis completely separated healthy volunteers and viral hepatitis B (VHB) induced liver fibrosis patients. Interestingly, the IVIM measurements of four VHB patients who showed no liver fibrosis by biopsy resembled those of healthy volunteers (12). Moreover, the signal difference between *b* =0 s/mm^2 image and very low *b* value image (such as *b* =1 or 2 s/mm^2) can be very substantial, the vessels (including small vessels) particularly show high signal without diffusion gradient while showing dark signal when the diffusion gradient is on even at *b* =1 s/mm^2; thus if the diffusion image signal decay is computed starting from *b* =0 s/mm^2 image and then increasingly higher *b* values, then this decay process may not follow a biexponential model for region of interest

(ROI) based analysis (13). In our two published studies we dealt this difficulty by ignoring the b =0 images, and take the assumption that the remaining signal *vs.* b value relationship follows a bi-exponential decay (11,13). This simplistic approach seems worked well in our published cases. However, in our two last studies, the starting b value for bi-exponential decay analysis was b =10 s/mm^2 and b =15 s/mm^2 respectively, thus very low b values were not available for computing IVIM parameters. This study has two primary aims. The first is to further confirm the diagnostic value of IVIM in detecting liver fibrosis. The second is to test whether by sampling very low b value densely, then b =0 s/mm^2 image could be included to improve IVIM's diagnostic performance for liver fibrosis detection.

Methods

This was a prospective study with MRI data acquired at the Third Xiangya Hospital of Central South University, Changsha, China. The study was approved by the institutional ethical committee of the Third Xiangya Hospital, and the informed consent was obtained for all the study subjects. Twenty-four healthy volunteers and 28 consecutive patients suspected of VHB induced liver fibrosis with liver biopsy results (pa1–pa20, and pb1–pb8), as well as 13 consecutive hepatocellular carcinoma (HCC) patients scheduled for surgery (pc1–pc13), were recruited. All the hepatocellular carcinoma patients had liver fibrosis. The biopsy and histology results of eight patients (pb1–pb8) was evaluated at the Second Xiangya Hospital of Central South University, while all other patients were evaluated at the Third Xiangya Hospital. For patients with chronic VHB, biopsy samples of ≥1.5 cm in length were taken from liver right lobe using 18-G sized needles under CT-guidance. For HCC patients, liver tissue adjacent to the resected tumor was processed for staging fibrosis and inflammation. The histology diagnosis and grading for liver fibrosis and inflammation was based on the widely accepted standard (METAVIR score for fibrosis) (14,15).

Magnetic resonance imaging (MRI) and liver biopsy or surgery were performed with less than 1-month interval. MRI was performed with a 3-T magnet with 32-channel abdominal phased-array coil (Ingenia, Philips Healthcare, Best, The Netherlands). In addition to standard clinical sequences, IVIM diffusion imaging was based on a single-shot spin-echo type echo-planar sequence, with 16 b values of 0, 2, 5, 10, 15, 20, 25, 30, 40, 60, 80, 100, 150, 200, 400, and 600 s/mm^2. Number of excitations (NEX) was 1 for b values of 0–150 s/mm^2, and NEX was 2 for 400 and 600 s/mm^2. SPIR technique (Spectral Pre-saturation with Inversion-Recovery) was used for fat suppression. Respiratory-gating was applied and resulted in an average TR of 871 ms, and the TE was 57 ms. Other parameters included matrix =116×119, field of view =350×372, slice thickness =6 mm, inter-slice gap =1.5 mm, number of slices =23. The data acquisition period was December 22, 2017 to December 13, 2018.

After MRI data acquisition, we performed a data quality assessment prior to IVIM analysis as described in our reports (12,16). Due to the factor that the balloon used for respiratory gating was found to be leaky when the study started, images of the initial three patients (pa1–pa3) and three of initial five volunteers (v1, v4, v5) were of insufficient image quality and thus excluded (*Figure S1*). During the remaining study period, one volunteer (v20) and four HCC patients were considered to have insufficient imaging quality (pc3, pc11–pc13), and two liver fibrosis patients had insufficient curve fitting quality (pa16, pb8) (*Figure S2*), resulting in a success rate of 95% (20/21) for volunteers and 84% (32/38) for patients.

After the exclusions described above, there were 20 healthy volunteers (10 males, 10 females; mean age: 28.3 years; range, 24–58 years), 4 patients had chronic VHB but biopsy did not show liver fibrosis (group-1, all with inflammation grade-1), 11 patients had stage-1 liver fibrosis (group-2), 10 patients had stage-2 liver fibrosis (group-3), and 2 and 5 patients respectively had stage-3 and stage-4 liver fibrosis (group-4). In the patient group, there were 24 males and 8 females, the mean age was 42.1 years (range, 21–65 years). In the liver fibrosis patients, 1 case had inflammation grade-0, 19 cases had inflammation grade-1, and 8 cases had inflammation grade-2. Overall, the correlation between fibrosis grading and inflammation grading was weakly positive (*Figure S3*).

All the study subjects' results were processed once by a trained reader (N Che-Nordin). For IVIM image processing, ROIs were placed to cover a large portion of right liver parenchyma while avoiding large vessels on b =2 s/mm^2 image (or on b =0 s/mm^2 image, or b =5 s/mm^2 image/ b =10 s/mm^2 image, see paragraphs below) of the selected b value image series, with large vessels locations checked on b =0 s/mm^2 image. With the consideration of respiration induced position shift of the same slice data acquisition during different b values, sufficient margins were allowed between the ROIs and the liver borders, large vessels and artifacts. ROIs were then copied and pasted on each

corresponding image of each *b* values. For ROI analysis, the IVIM parameters were calculated based on the mean signal intensity of the whole ROIs, which offers better estimation than pixel-wise fitting when the signal-to-noise ratio (SNR) of images is low (17,18). The mean signal intensity of each ROI was weighted by the number of pixels included in each ROI, then the average of the weighted mean signal intensity of individual slice's ROIs was calculated to obtain the average signal value of the liver.

Curve-fitting algorithms were implemented in a custom program developed on MATLAB (Mathworks, Natick, MA, USA). Based on our recent experiences (11-13), the analysis was performed with b =2 s/mm^2 image as the starting point, and segmented fitting with a threshold-b (*Sbb*) of 60 s/mm^2 was selected. The signal value at each b value was normalized by attributing a value of 100 at b =2 s/mm^2 [S_{norm} = (SI/SI_2) ×100, where S_{norm} is the normalized signal, SI = signal at a given b value, and SI_2 = signal at b =2 s/mm^2]. For bi-compartmental model, the signal attenuation was modeled according to Eq. [1]:

$$SI(b) = SI_2 \times [(1 - PF) \times \exp(-b \times D_{slow}) + PF \times \exp(-b \times D_{fast})] \quad [1]$$

where SI(b) and SI_2 denote the signal intensity acquired with the b-factor value of b and b =2 s/mm^2, respectively (13).

For segmented fitting, the estimation of Dslow was obtained by a least-square linear fitting of the logarithmized image intensity at *Sbb*-values greater than 60 s/mm^2 to a linear equation. The fitted line was then extrapolated to obtain an intercept at b =2 s/mm^2, and the ratio between this intercept and SI_2 gave an estimate of PF. Finally, the obtained Dslow and PF were substituted into Eq. [1] and non-linear least-square fitted against all b values to estimate Dfast using Trust-Region algorithm (*Figure 1*).

As noted above, in this study the reference results were the results computed using segmented fitting with *Sbb* =60 s/mm^2 and starting from b =2 s/mm^2 (Analysis-1). These results were then compared with results of: (I) using segmented fitting with *Sbb* =40 s/mm^2 and starting from 2 s/mm^2 (Analysis-2); (II) full fitting started from b =2 s/mm^2 (Analysis-3); (III) using segmented fitting with *Sbb* =60 s/mm^2 and starting from b =0 s/mm^2 (Analysis-4); (IV) using segmented fitting with *Sbb* =40 s/mm^2 and starting from b =0 s/mm^2 (Analysis-5); (V) using segmented fitting with *Sbb* =60 s/mm^2 and starting from b =5 s/mm^2 (excluding b =0 and 2 s/mm^2) (Analysis-6); (VI) using segmented fitting with *Sbb* =60 and starting from b =10 s/mm^2 (excluding b =0, 2 and =5 s/mm^2) (Analysis-7). For the analysis starting from b =0, 5 s/mm^2, the ROIs drawn on b =2 s/mm^2 images were saved and reloaded for processing. For the analysis starting from b =10 s/mm^2, new ROIs were also drawn based on b =10 s/mm^2 images, and the IVIM parameter results based on the new ROIs and results based on ROIs of b =2 s/mm^2 was compared and found they were broadly similar. Results based on the new ROIs on b =10 s/mm^2 images were used to compare with other methods' results.

For IVIM analysis methods comparison, two aspects were considered: (I) standard deviation and coefficient of variation (CoV) for healthy volunteers, and (II) the mean measurement for a patient group divided by the mean measurement for healthy volunteers [denoted as patient/volunteer (pt/vol) ratio in this study]. Taking the assumption that IVIM measurement variations among the healthy volunteers are more likely due to measurement imprecision rather than genuine physiological difference among the volunteers, then the computing method resulting in a smaller CoV is favored. The smaller the pt/vol ratio, the bigger the difference between the measurements for patients' value and healthy volunteers' value (if there is no difference between the mean value of healthy subjects and mean value of patients, then pt/vol ratio is 1); therefore, the computing approach resulting in a smaller pt/vol ratio is favored. In addition, among the three IVIM parameters, smallest pt/vol ratio and smallest CoV for PF will be favored, as PF offers the best diagnostic value for separating healthy volunteers and patients. The separations of healthy subjects and patient subjects were also visually assessed by a 3D tool. This 3D tool was programed using IBM SPSS 23 for Windows (SPSS Inc., Chicago, IL, USA), and the measurements of Dslow, PF, and Dfast were placed along the x-axis, y-axis, and z-axis (11). While the pt/vol ratio provide the mean separation between two groups, the 3D tool provided assessment for extreme values and outliers.

To investigate the potential correlation between IVIM readouts and liver function, three IVIM parameters derived from Analyses-1–7 were plotted against serum liver function biomarkers of total protein, albumin, alanine transaminase (ALT), aspartate transaminase (AST), total bilirubin and direct bilirubin. As this part of analysis was not statistically planned, emphasis was focused on the visual inspection of the graphs for potential correlation. Serum liver function biomarkers were not available for the healthy volunteers.

To assess the inter-reader ROI-based measurement's

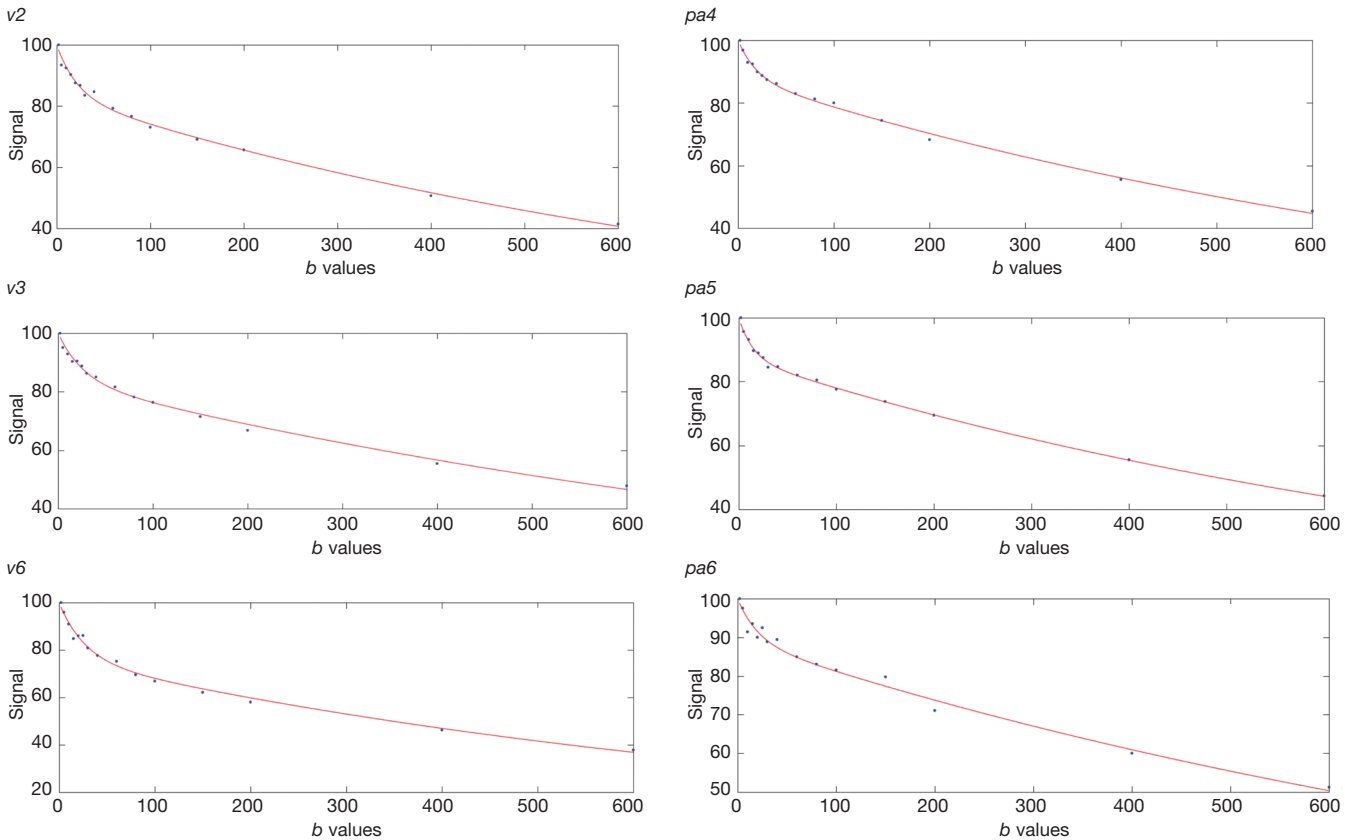

Figure 1 Bi-exponentially fitted curves from the first included three volunteers and first included three patients. The starting *b* value is 2 s/mm^2 and the threshold *b* value is 60 s/mm^2. The fitting curve of subject pa6 was considered acceptable as the deviated values are distributed symmetrically both below and above the fitting curve.

reproducibility, 14 randomly selected patients (5 VHB patients and 9 HCC patients) were measured independently again by a radiology trainee (SW Qiu) who received a short period of training on how to draw ROI on liver parenchyma.

Results

The intraclass correlation coefficient (ICC) for inter-reader measurement reproducibility was 0.969, 0.95, and 0.83, for PF, Dfast and Dslow respectively, thus indicating good measurement reproducibility (*Table S1*).

The comparison of the seven analysis methods for healthy volunteers is shown in *Table 1*. As expected, *Sbb* =40 s/mm^2 was associated with slightly higher Dslow value compared with values computed with *Sbb* =60 s/mm^2. The smaller starting *b* values for bi-exponential analysis, and more so for *b* =0 s/mm^2, were associated with larger PF and Dfast values. Among the seven analysis methods, Analysis-1 showed the smallest CoV for all PF, Dfast, and Dslow, thus the healthy volunteers data favored Analysis-1. The comparison of the seven analysis methods for three groups of patients is shown in *Table 2*. Analysis-1 showed the smallest pt/vol ratio for PF of F2 group and F3–4 group, smallest pt/vol for all three groups' Dslow, smallest CoV for F2 group's PF, and second smallest CoV for F1 group's PF. Analysis-7 showed the smallest pt/vol ratio for F1 group's PF, and the second smallest Dfast pt/vol for F1 group and the smallest Dfast pt/vol for F2 group. However, Analysis-7 was associated with relatively large CoVs. Thus, the following analyses were primarily performed using Analysis-1 data, and assisted by Analysis-7 when Analysis-7 showed advantages.

Using Analysis-1, the individual volunteers' and patients' data are shown in *Tables 3*,*S2*,*S3* and graphically in *Figure 2*. The IVIM measures of four patients without liver fibrosis

Table 1 IVIM parameters of healthy volunteers computed by seven data processing methods

Methods	PF[#]	Dfast[#]	Dslow[#]
Anal1: seg fitting, *Shb60*, *b* =2~	0.167±0.025, 0.148*	44.4±8.8, 0.20*	1.16±0.08, 0.07*
Anal2: seg fitting, *Shb40*, *b* =2~	0.152±0.031, 0.207	47.6±10.9, 0.23	1.18±0.11, 0.09
Anal3: full fitting, *b* =2~	0.167±0.038, 0.228	43.2±13.6, 0.31	1.14±0.11, 0.10
Anal4: seg fitting, *Shb60*, *b* =0~	0.280±0.051, 0.181	178.3±75.3, 0.42	1.15±0.11, 0.09
Anal5: seg fitting, *Shb40*, *b* =0~	0.273±0.051, 0.185	200.5±79.7, 0.40	1.17±0.11, 0.09
Anal6: seg fitting, *Shb60*, *b* =5~	0.122±0.031, 0.256	26.3±5.9, 0.23	1.15±0.11, 0.09
Anal7: seg fitting, *Shb60*, *b* =10~	0.103±0.029, 0.278	18.5±4.0, 0.22	1.16±0.11, 0.09

[#], mean ± standard deviation, CoV; *, denote smallest CoV. *Shb60*: threshold *b* =60 s/mm^2; *b* =2~: curve fitting starting from *b* =2 s/mm^2; *b* =0~: curve fitting starting from *b* =0 s/mm^2. Dfast and Dslow in $\times 10^{-3}$ mm^2/s. CoV, coefficient of variation; IVIM, intravoxel incoherent motion; Anal1, Analysis-1; seg fitting, segmented fitting.

Table 2 Comparison of measure of patients' value divided by volunteers' value for IVIM parameter by seven analysis methods

Variables	PF			Dfast			Dslow		
	F1	F2	F3-4	F1	F2	F3-4	F1	F2	F3-4
pt/vol1	0.701	0.753[#]	0.627[#]	1.14	1.14	0.842	0.864[#]	0.879[#]	0.845[#]
pt/vol2	0.752	0.869	0.686	0.859[#]	1.15	0.895	0.893	0.892	0.882
pt/vol3	0.698	0.845	0.771	1.294	1.22	0.796	0.921	0.915	0.864
pt/vol4	0.822	0.983	0.710	1.367	1.44	0.783[#]	0.903	0.902	0.874
pt/vol5	0.829	0.987	0.709	1.301	1.40	0.784	0.895	0.900	0.871
pt/vol6	0.705	0.892	0.824	1.284	1.10	1.09	0.901	0.897	0.904
pt/vol7	0.592[#]	0.796	0.681	0.967*	0.934[#]	0.865	0.897*	0.895	0.918
CoV1	0.147*	0.274[#]	0.179	0.254	0.214	0.301	0.060	0.076	0.144
CoV2	0.141[#]	0.292	0.301	0.232[#]	0.139[#]	0.310	0.057[#]	0.061[#]	0.100
CoV3	0.181	0.301	0.301	0.267	0.231	0.466	0.064	0.070	0.115
CoV4	0.158	0.294	0.107[#]	0.315	0.444	0.470	0.063	0.062	0.104
CoV5	0.152	0.294	0.110	0.300	0.414	0.452	0.057[#]	0.059	0.105
CoV6	0.237	0.390	0.345	0.237	0.210	0.212[#]	0.063	0.068	0.096
CoV7	0.326	0.312	0.148	0.428	0.199	0.272	0.059	0.063	0.097[#]

[#], indicates the smallest value in the group; *, the second smallest value in the group. pt/vol1: pt/vol ratio of the group (F1, or F2 or F3–4) computed with Analysis-1 method; CoV1: coefficient-of-variation of the group computed with Analysis-1 method. IVIM, intravoxel incoherent motion; pt/vol, patient/volunteer.

resembled those of healthy subjects. PF offered the best diagnostic value for separating healthy livers and fibrotic livers, and a threshold of 0.1406 separated all fibrotic livers and healthy livers with an exception of patient-C1 (a HCC patient with fibrosis grade-2/inflammation grade-2). C1's PF, Dfast, and Dslow were 0.199, 47.5, and 1.01 respectively, all well within the range of healthy livers (*Table 3*). *Figure 2* shows that there was no notable difference in the means of (all) PF, Dslow, and Dfast among the three fibrotic liver groups. Dfast offered little value in separating healthy livers from fibrotic livers, though the mean Dfast of F3–4 group was smaller than the other four groups. *Figure 2D*

Table 3 Mean, standard deviation (SD), of PF, Dslow, and Dfast of healthy volunteers, patients without liver fibrosis (F0), stage 1 liver fibrosis (F1) patients, stage 2 liver fibrosis (F2) patients, and stage 3–4 liver fibrosis (F3–4) patients

Variables	PF	Dfast ($\times 10^{-3}$ mm^2/s)	Dslow ($\times 10^{-3}$ mm^2/s)
Healthy	0.167±0.025	44.4±8.8	1.16±0.08
Patients F0	0.158±0.012	48.1±3.0	1.12±0.03
Patients F1	0.117±0.017	50.5±12.8	1.00±0.06
Patients F2	0.126±0.035	50.5±10.8	1.02±0.08
Patients F3–4	0.105±0.019	37.4±11.3	0.98±0.14

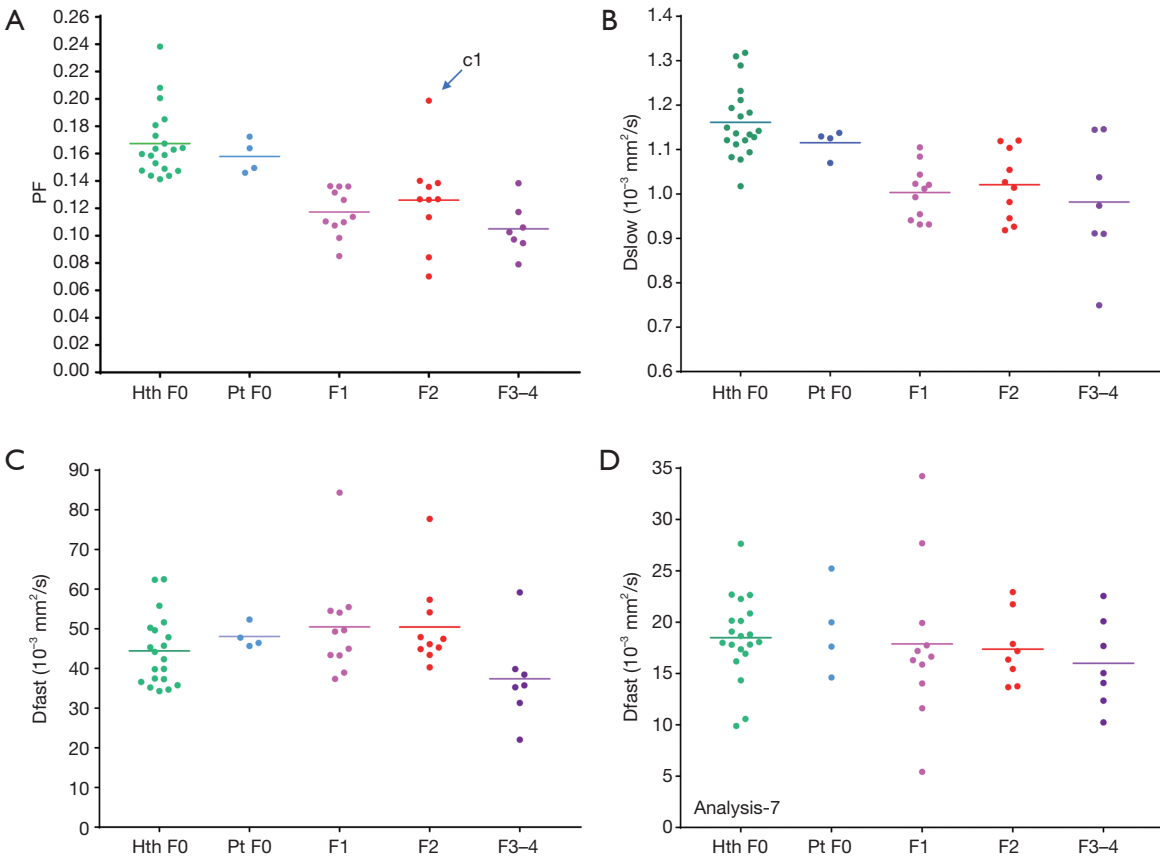

Figure 2 Scattered plots and mean of PF (A), Dslow (B), and Dfast (C,D) of healthy volunteers (HthF0), patients without liver fibrosis (PtF0), stage-1 liver fibrosis (F1) patients, stage-2 liver fibrosis (F2) patients, and stage 3–4 liver fibrosis (F3–4). The starting *b* value is 2 s/mm^2 for (A,B,C), and 10 s/mm^2 for (D), the threshold b value is 60 s/mm^2 for all cases (A,B,C,D).

shows the Dfast values when Analysis-7 was applied, with a weak trend of more severe liver fibrosis associated with lower Dfast. *Figure 3* shows, compared with fibrotic livers with inflammation grade-1, fibrotic livers with inflammation grade-2 showed a trend of higher Dfast.

Figure 4 shows 3D display of healthy volunteer group (green dots), patients without liver fibrosis group (yellow dots), liver fibrosis patient group (red dots). The differentiation of volunteers group and liver fibrosis patient group can be visualized by rotating in 3D space (dotted yellow line). The distribution of patients without liver fibrosis resembled healthy volunteers. Patient-C1 was in the

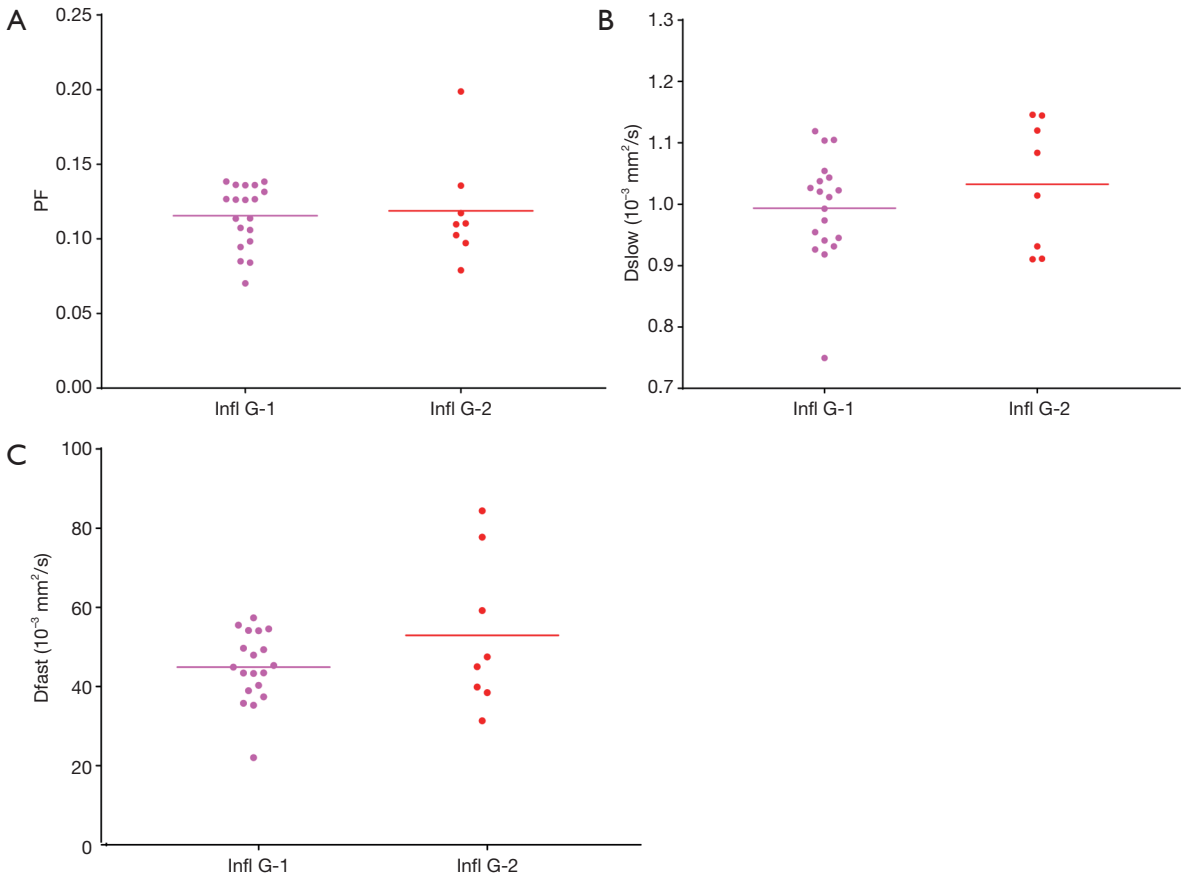

Figure 3 Scattered plots and mean of PF (A), Dslow (B), and Dfast (C) for inflammation grade-1 cases (n=19) and grade-2 cases (n=8) with liver fibrosis. Patients without fibrosis and one fibrosis patient with inflammation grade-0 was not included here. The starting *b* value is 2 s/mm^2, the threshold *b* value is 60 s/mm^2. Infl G1, inflammation grade-1; Infl G2, inflammation grade-2.

healthy volunteer cluster.

Figure 5 shows potential correlation between PF/Dfast and serum liver function biomarkers. Weak correlation is shown with lower PF and lower Dfast associated with lower total protein, lower albumin; higher ALT, higher AST; higher total bilirubin, and higher direct bilirubin. No correlation was noted with Dslow and serum liver function biomarkers. Visual inspection showed, as compared with Analyses-2–6, the correlations between PF/Dfast and serum liver function biomarkers were better demonstrated with Analysis-1 or Analysis-7.

Discussion

IVIM diffusion imaging has the promise of obtaining *in-vivo* tissue perfusion/diffusion (PD) information non-invasively. However, its clinical diagnostic application at individual patient's level has been challenging (10). In this study, the reference method was to compute IVIM results using segmented-fitting with *Shb* =60 s/mm^2 and starting from *b* =2 s/mm^2 (Analysis-1), and this method was compared with six other analysis methods (Analyses-2–7), representing our efforts to test and fine-tune data acquisition and data-post processing so to optimize these procedures. It can be expected that the experiences learned for liver fibrosis evaluation can also be useful for IVIM analysis of other pathologies and other organs, particularly perfusion-rich tissues. We recently argued that the commonly used IVIM analysis, where the diffusion image signal decay is computed starting from *b* =0 s/mm^2 image and then increasingly higher *b* values using a bi-exponential decay model, may not be valid as this decay process may not follow a bi-exponential model for ROI-based analysis (13). A simplistic approach ignoring *b*=0 s/mm^2 image seems worked

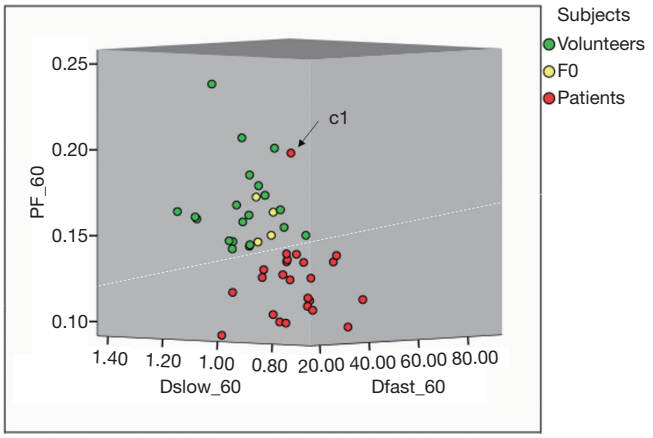

Figure 4 3D display of healthy volunteer group (green dots), patients without liver fibrosis group (yellow dots), liver fibrosis patient group (red dots). Each dot represents one participant. The differentiation of volunteer group and liver fibrosis patient group can be visualized by rotating in 3D (dotted yellow line) except patient-C1. Note the distribution of four viral hepatitis B patients without liver fibrosis resembles healthy volunteers.

well in our published series (11,12). The current study further confirmed that data analysis without b =0 s/mm^2, particularly starting from b =2 s/mm^2, outperformed data analysis where b =0 s/mm^2 was included (Analyses-4 & 5). Since in our last two reports we used 10 and 15 s/mm^2 as the starting lowest b value for bi-exponential analysis, in this study we tested if the addition of b =2 s/mm^2 and b =5 s/mm^2 would improve the diagnostic performance. This study indeed suggests that addition of b =2 s/mm^2 and b =5 s/mm^2 has improved the diagnostic performance compared with analysis using b =10 s/mm^2 as the lowest b value for analysis.

This study shows that, overall, IVIM results using segmented-fitting with *Sbb* =60 s/mm^2 and starting from b =2 s/mm^2 (Analysis-1) presented the best results compared with the other six methods; while Analysis-7, segmented-fitting starting from b =10 s/mm^2, showed some advantages in computing Dfast (*Figures 2D,5*). We argued that the selection of signal decay model and fitting model may depend on the pathologies to be studied, multiple model analyses can be applied for the same pathology (19). We have shown that *Sbb* =60 s/mm^2 maximizes the distance between healthy livers data cluster and fibrotic livers cluster (20). While the difference between data computed with *Sbb* =40, 60, or 80 s/mm^2 was not big, the difference between data computed with *Sbb* =60 and 200 s/mm^2 was substantial (20). We also reported better scan-rescan repeatability and scan-rescan reproducibility for both PF and Dslow when *Sbb* =50 or 80 s/mm^2 as compared with when *Sbb* = 200 s/mm^2 (16). Our more recent study also confirmed that *Sbb* =60 s/mm^2 outperforms *Sbb* =200 s/mm^2 for separating healthy livers and fibrotic livers (12). However, the lowest starting b value for IVIM analysis in those two studies was 10 and 15 s/mm^2 respectively (11,12). Since in the current study lower b values of 2 and 5 s/mm^2 were sampled, it would be theoretically possible a *Sbb* lower than 60 s/mm^2 might work better for separating healthy livers and fibrotic livers. However, this study shows that, when the lowest b value for analysis was 2 s/mm^2, *Sbb =60* s/mm^2 remained performing better than *Sbb* =40 s/mm^2. The limitations of full-fitting method have been previously noted. Park *et al.* (21) showed that full-fitting, particularly when used without constrains, may result in a large measurement error and a poor reliability of IVIM parameters when the image SNR is low. As the full-fitting method simultaneously fits all three parameters using a nonlinear least-square fitting algorithm, bad data points due to image noise may have led to erroneous fitting results, particularly when used without constrains, which can be exacerbated in low SNR settings. The segmented-fitting method, which estimates each IVIM parameter step-by-step, improves the reliability of IVIM parameters. Park *et al.* (21) suggested that for diffusion image data with a limited number of b values and a low SNR, segmented fitting methods should be preferred over full-fitting methods.

The same as our previous studies (11,12), this study shows, among the three IVIM parameters, PF showed the best diagnostic performance. However, the Dfast value calculated with analysis-1 did not meet our pre-study expectation. Despite we added very low b =2, 5 s/mm^2, the diagnostic performance of Dfast was not good in this study (*Figure 2C*). This is likely due to the inclusion of these very low b values lead to the inclusion of the initial very fast decay for analysis; however, to quantify the initial very fast decay, very low b values remained insufficient even after b =2, 5 s/mm^2 were added, thus Dfast's variation among individuals increased. Even more very low b values may be required to reduce errors in Dfast estimation (22). Analysis-7 with fitting starting from b =10 s/mm^2 showed a weak trend that the mean value of Dfast is lower in advanced fibrosis than milder fibrosis (*Figure 2D*). Analysis-7 also showed some advantages for correlations with serum liver function biomarkers (*Figure 5*). Though

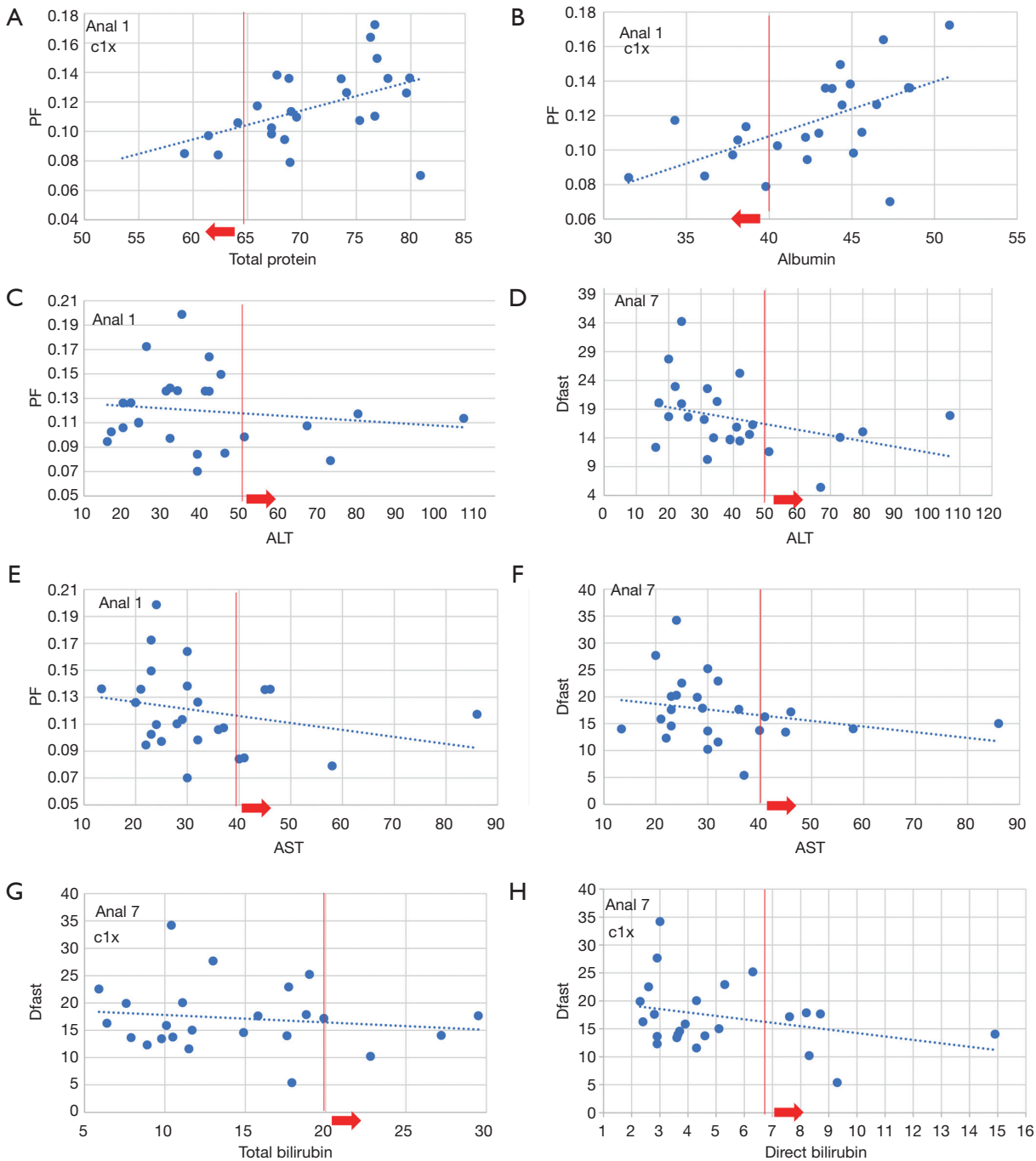

Figure 5 Potential correlation between IVIM readouts (PF and Dfast) and serum liver function biomarkers. Vertical redline separates normal range and abnormal values which is further marked by red arrow. (A) potential positive correlation between PF and total protein (normal range, 65–85 g/L); (B) potential positive correlation between PF and albumin (normal range, 40–55 g/L); (C) potential negative correlation between PF and ALT (normal range, 9–50 U/L); (D) potential negative correlation between Dfast and ALT; (E) potential negative correlation between PF and AST (normal range, 15–40 U/L); (F) potential negative correlation between Dfast and AST; (G) potential negative correlation between Dfast and total bilirubin (normal range, 3.42–20.5 μmol/L), note subjects with total bilirubin >20 had low Dfast; (H) potential negative correlation between Dfast and direct bilirubin (normal range, 0–6.81 μmol/L); Anal-1, Analysis-1 method; Anal-7, Analysis-7 method; c1x, patient-c1 was excluded from analysis; ALT, alanine transaminase; AST, aspartate transaminase.

for the fibrotic livers of the current study, PF alone provides sufficient separation between healthy subjects and patients, it is expected analysis incorporating all three IVIM parameters would be useful for marginal cases (11).

Fibrosis, regenerative nodule formation, and intrahepatic vasoconstriction are classical mechanisms that account for increased intrahepatic vascular resistance in cirrhosis. Mechanisms responsible for the increase in sinusoid resistance include a mechanic factor which is a direct consequence of fibrosis deposition and a dynamic component related to endothelial dysfunction, deficient intrahepatic nitric oxide production, increased vasoconstrictor production, and other factors that promote the increased contraction of hepatic stellate cells (23-25). The results of our three studies, including this study and two recently reported studies (11,12), and numerous previous group-wise reports suggest the majority of fibrotic livers have decreased PD (10). This study showed four chronic VHB patients without fibrosis had IVIM measures resembled those of healthy volunteers, which supports our recent report that patients of chronic VHB without fibrosis could have normal liver PD (12). However, there was one apparent patient outlier, i.e., patient-C1 (fibrosis stage-2/ inflammation stage-2) in this study. The image quality and fitting curve of this patient were quite acceptable (*Figure S4*). We additionally performed a preliminary analysis of the liver parenchyma signal difference between sb0 (signal at b =0 image) and sb2 (signal at b =2 image). This patient had (sb0 – sb2)/ROIarea =65.4 and (sb0 – sb2)/sb2 =0.29, indicating rich blood vessel density of liver parenchyma (13). IVIM measures the PD status of liver, rather than the histological structure and collagen deposition of fibrotic liver, it is not really unusual that some livers with fibrosis may have PD measures in normal range, particularly if apparent inflammation is present.

Though our results suggest IVIM results alone can contribute to a very large extent in separating healthy livers and fibrotic livers, and advanced stage liver fibrosis shows more disturbed PD than early stage liver fibrosis, IVIM has not been good at separating fibrotic livers into different severity groups defined by histopathological grading. This can be partially due to the imprecision of liver IVIM measurement and partially due to the tissue sampling bias and subjectivity of histopathological assessment. It is also highly probable that IVIM measures do not necessarily agree with histopathological grading at one-to-one individual patients' level. This point has been suggested by previous CT perfusion studies (8,26,27). Thaiss *et al.* (26) reported portal-venous perfusion measured by CT was higher in liver fibrosis than in complete liver cirrhosis; however, they did not found correlation between perfusion CT parameters and Child-Pugh score or the clinical laboratory values. With perfusion CT, Ronot *et al.* (27) demonstrated that, compared with those with minimal fibrosis (F1), patients with intermediate fibrosis (F2 and F3) had decreased portal venous perfusion and total liver perfusion, while the mean transit time increased. Multivariate analysis showed only mean transit time was an independent factor; however, mean transit time allowed discrimination between minimal and intermediate fibrosis with a sensitivity of only 71% and a specificity of only 65%. Van Beers *et al.* (8) reported that perfusion CT demonstrated liver perfusion was decreased and mean transit time was increased in patients with cirrhosis; however, there were substantial overlaps among control subjects, patients with noncirrhotic chronic liver disease, and patients with liver cirrhosis. The correlation between severity of liver disease categorized in five classes (normal, noncirrhotic chronic liver disease, liver cirrhosis Child A, liver cirrhosis Child B, liver cirrhosis Child C) and perfusion CT parameters was only modest (8).

Previous studies showed that the presence of interface hepatitis in initial biopsies from patients with chronic viral hepatitis C correlates with subsequent development of cirrhosis; and an association between the severities of necroinflammatory activity in an initial biopsy and the development of fibrosis or cirrhosis in follow up biopsies (14). As expected, a weak positive association was noted between fibrosis grading and inflammation grading (*Figure S3*). In addition to fibrosis, the coexisting inflammation is likely to also influence liver PD.

This study shows a trend that, grade-2 inflammation might be associated with higher liver perfusion as compared with grade-1 inflammation (*Figure 3*). In interpreting *Figure 3*, it should be noted that, since higher grade of inflammation is (weakly) associated higher grade of fibrosis and liver fibrosis is associated with a decrease of PF, Dfast and Dslow (10,11), then if inflammation does not influence PD, grade-2 inflammation livers would demonstrate lower IVIM parameters. For example, since *Figure 3* shows grade-1 inflammation livers and grade-2 inflammation livers had similar mean PF values, it is likely that inflammation might have already promoted higher PF. The interplay between fibrosis and inflammation might have complicated the relation between fibrosis severity and the amount of Dfast decrease.

The correlation between IVIM readouts of PF and Dfast

and serum liver function biomarkers was noted in this study; however, these correlations were neither strong nor "clean". Both IVIM readouts and liver function biomarkers have the measurement imprecision issue. In one study, Lazo *et al.* (28) reported that elevated AST, ALT, or bilirubin levels were reclassified as normal in more than 30% of retested individuals. γ-glutamyltransferase and alkaline phosphatase had approximately 15% of adults being reclassified as having normal levels after initially abnormal test results. On the other hand, these results could be unchanged, even after alcohol use, hepatitis infection status, and use of medications known to be hepatotoxic were taken into account. Fasting time can induce another variable for liver function serum biomarkers (29). Note patients with liver fibrosis do not necessarily demonstrate abnormal serum liver function biomarkers. In our study, serum liver function biomarkers were still in normal range for >50% of the patients. Therefore, it is not surprising that the correlation between IVIM readouts of PF and Dfast and serum liver function biomarkers were weak in this study. This study did not show correlation between Dslow and serum liver function biomarkers.

The correlation between IVIM readouts of PF and Dfast and liver fibrosis staging should also be viewed with the consideration that liver biopsy is an imperfect method to diagnose liver fibrosis. Needle liver biopsy has been shown to have a high rate of sampling error in patients with diffused parenchymal liver diseases. A liver biopsy samples only 1/50,000th of the liver parenchyma, as such the sample of liver tissue may not necessarily reflect the true degree of inflammation, fibrosis, or cirrhosis (30). Sampling errors even occur despite an adequate sample size and a satisfactory number of portal tracts. Regev *et al.* (31) reported a comparison between the right and left lobes yielded a difference of at least one stage of fibrosis in as many as 33.1% of viral hepatitis C patients, although differences greater than one stage or grade were uncommon. In addition, interpretation of cirrhosis was given in one lobe but not in the other in 14.5% cases. When grades of necroinflammatory activity were compared, a difference of at least one grade between the right and left lobes was found in 24.2% of the patients. Poynard *et al.* once proposed this question: Is there a true gold standard for liver fibrosis (32,33)? Non-invasive imaging has the advantage that it can potentially examine the whole liver with good spatial resolution.

This study has several limitations. All our patients had liver fibrosis due to VHB, whether results of our study can be generalized to liver fibrosis of other causes remains to be validated. Chronic liver disease causes include chronic viral hepatitis, alcohol, non-alcoholic fatty liver disease (NAFLD), hemochromatosis, alpha-1 antitrypsin deficiency, and cholestatic and autoimmune diseases. NAFLD is expected to rise with the high prevalence of obesity and type-2 diabetes worldwide (34). The detection of liver fibrosis in NAFLD is of high clinical importance as liver fibrosis is the single most important factor that determines long-term outcome in NAFLD patients (35). Since this study shows the addition of very low *b* values improved the diagnostic performance of liver IVIM, we assume there is still room for improvement with the *b* values used in this study; for example, we may include more very low *b* values such as 2, 3, 5, 8, 10 s/mm^2 for future studies. This may be important as in this study Dfast alone performed poorly in separating healthy livers and fibrotic livers. When this study was started, the radiographers at the Changsha site were not experienced in performing IVIM data acquisition, so that the images of the first three patients and three of the first five volunteers were of all insufficient quality. Excluding the initial three volunteers and three patients, 95% (20/21) of volunteers and 84% (32/38) of patients had sufficient IVIM image quality for analysis. This success rate is similar to our recent experience (12). We expect as the radiographers gain experiences in acquiring IVIM images, the success rate is likely to increase. Moreover, the TR (=871 ms) used for IVIM was quite short in this study, so that the image quality as assessed subjectively was generally inferior to our previous studies performed in Shenzhen (TR =1,600 ms) and Nanjing (TR =2,149 ms) (11,12,16). The slice thickness (=6 mm) used in this study was also slightly thinner than our previous studies (Shenzhen, =7 mm). As this study was planned to be exploratory, we did not emphasize the statistics, instead we paid more attentions to the trends demonstrated in the results. We may leave the statistics to the final large-scale study or meta-analysis. Another limitation of this study is that our volunteers were younger than the patients. Lastly, as post-meal and fasted status may influence blood flow to the liver, it can be recommended in the future that all patients should fast for 6 hours before the MRI procedure (36).

In conclusion, we compared seven IVIM data analysis methods, and the results suggest that segmented-fitting with *Shb* =60 s/mm^2 and starting from non-zero very low *b* value (*b* =2 s/mm^2 in this study) outperformed other methods. Since our *b* value distribution might not have

offered most reliable Dfast estimation, this study also showed segmented-fitting starting from a low *b* value of 10 s/mm^2 was useful in some circumstances. This study further confirms the practical appropriateness of excluding *b* =0 s/mm^2 for bi-exponential decay analysis, even two very low *b* values (*b* =2 and 5 s/mm^2) were sampled in this study. This study demonstrates that IVIM has high sensitivity in detecting liver fibrosis, and PF and Dfast have potential correlation with serum liver function biomarkers. However, IVIM measures and liver fibrosis grading are not in a linear relationship, and this may also be complicated by that higher-grade liver inflammation might be associated with higher Dfast measure. In combination of our recent two studies, our data suggest that IVIM measures can be independent biomarkers for evaluating liver pathophysiology (37). In the meantime, we acknowledge that the liver IVIM data acquisition and post-processing methods remain to be further optimized.

Acknowledgements

Funding: This work was partially supported by grants from the National Natural Sciences Foundation of China (No. 81471715 and 81771827), Natural Sciences Foundation of Hunan province (No. 2017JJ2369), and a grant from the Research Grants Council of Hong Kong SAR (Project No. 2141061).

Footnote

Conflicts of Interest: The authors have no conflicts of interest to declare.

Ethical Statement: The study was approved by the institutional ethical committee of the Third Xiangya Hospital, and the informed consent was obtained for all the study subjects.

References

1. GBD 2015 Mortality and Causes of Death Collaborators. Global, regional, and national life expectancy, all-cause mortality, and cause-specific mortality for 249 causes of death, 1980-2015: a systematic analysis for the Global Burden of Disease Study 2015. Lancet 2016;388:1459-544.
2. Marcellin P, Gane E, Buti M, Afdhal N, Sievert W, Jacobson IM, Washington MK, Germanidis G, Flaherty JF, Aguilar Schall R, Bornstein JD, Kitrinos KM, Subramanian GM, McHutchison JG, Heathcote EJ. Regression of cirrhosis during treatment with tenofovir disoproxil fumarate for chronic hepatitis B: a 5-year open-label follow-up study. Lancet 2013;381:468-75.
3. D'Ambrosio R, Aghemo A, Rumi MG, Ronchi G, Donato MF, Paradis V, Colombo M, Bedossa P. A morphometric and immunohistochemical study to assess the benefit of a sustained virological response in hepatitis C virus patients with cirrhosis. Hepatology 2012;56:532-43.
4. Campana L, Iredale JP. Regression of liver fibrosis. Semin Liver Dis 2017;37:1-10.
5. Patel K, Shackel NA. Current Status of Fibrosis Markers. Curr Opin Gastroenterol 2014;30:253-9.
6. Moreno AH, Burchell AR, Rousselot LM, Panke WF, Slafsky F, Burke JH. Portal Blood Flow in Cirrhosis of the Liver. J Clin Invest 1967;46:436-45.
7. Iwakiri Y, Groszmann RJ. The Hyperdynamic Circulation of Chronic Liver Diseases: from the Patient to the Molecule. Hepatology 2006;43:S121-S131.
8. Van Beers BE, Leconte I, Materne R, Smith AM, Jamart J, Horsmans Y. Hepatic Perfusion Parameters in Chronic Liver Disease: Dynamic CT Measurements Correlated with Disease Severity. AJR Am J Roentgenol 2001;176:667-73.
9. Blendis L, Wong F. The Hyperdynamic Circulation in Cirrhosis: An Overview. Pharmacol Ther 2001;89:221-31
10. Li YT, Cercueil JP, Yuan J, Chen W, Loffroy R, Wáng YX. Liver intravoxel incoherent motion (IVIM) magnetic resonance imaging: a comprehensive review of published data on normal values and applications for fibrosis and tumor evaluation. Quant Imaging Med Surg 2017;7:59-78.
11. Wáng YX, Deng M, Li YT, Huang H, Leung JCS, Chen W, Lu PX. A Combined Use of Intravoxel Incoherent Motion MRI Parameters Can Differentiate Early-Stage Hepatitis-b Fibrotic Livers from Healthy Livers. SLAS Technol 2018;23:259-68.
12. Huang H, Che-Nordin N, Wang LF, Xiao BH, Chevallier O, Yun YX, Guo SW, Wáng YX. High performance of intravoxel incoherent motion diffusion MRI in detecting viral hepatitis-b induced liver fibrosis. Ann Transl Med 2019;7:39.
13. Wang YX. Living tissue intravoxel incoherent motion (IVIM) diffusion MR analysis without b=0 image: an example for liver fibrosis evaluation. Quant Imaging Med Surg 2019;9:127-33.
14. Shiha G, Zalata K. Chapter 10: Ishak versus METAVIR:

Terminology, Convertibility and Correlation with Laboratory Changes in Chronic Hepatitis C (page 155-170). In: Takahashi H. editor. Liver Biopsy. Rijeka (Croatia): InTech, 2011:155-70.
15. Bedossa, P, Poynard T. An Algorithm for the Grading of Activity in Chronic Hepatitis C. The METAVIR Cooperative Study Group. Hepatology 1996;24:289-93.
16. Chevallier O, Zhou N, He J, Loffroy R, Wáng YX. Removal of evidential motion-contaminated and poorly fitted image data improves IVIM diffusion MRI parameter scan-rescan reproducibility. Acta Radiol 2018;59:1157-67.
17. Yuan J, Wong OL, Lo GG, Chan HH, Wong TT, Cheung PS. Statistical assessment of bi-exponential diffusion weighted imaging signal characteristics induced by intravoxel incoherent motion in malignant breast tumors. Quant Imaging Med Surg 2016;6:418-29.
18. Li YT, Huang H, Zhuo Z, Lu PX, Chen W1, Wáng YX. Bi-phase age-related brain gray matter magnetic resonance T1r relaxation time change in adults. Magn Reson Imaging 2017;39:200-5.
19. Chevallier O, Zhou N, Cercueil JP, He J, Loffroy R, Wang YX. Comparison of tri-exponential decay vs. bi-exponential decay and full fitting vs. segmented fitting for modeling liver intravoxel incoherent motion diffusion MRI. bioRxiv 2018. Available online: http://dx.doi.org/10.1101/429977
20. Wáng YX, Li YT, Chevallier O, Huang H, Leung JCS, Chen W, Lu PX. Dependence of intravoxel incoherent motion diffusion MR threshold b-value selection for separating perfusion and diffusion compartments and liver fibrosis diagnostic performance. Acta Radiol 2019;60:3-12.
21. Park HJ, Sung YS, Lee SS, Lee Y, Cheong H, Kim YJ, Lee MG. Intravoxel incoherent motion diffusion-weighted MRI of the abdomen: The effect of fitting algorithms on the accuracy and reliability of the parameters. J Magn Reson Imaging 2017;45:1637-47.
22. Zhang Q, Wang YX, Ma HT, Yuan J. Cramér-Rao bound for Intravoxel Incoherent Motion Diffusion Weighted Imaging Fitting. Conf Proc IEEE Eng Med Biol Soc 2013;2013:511-4.
23. Thabut D, Shah V. Intrahepatic angiogenesis and sinusoidal remodeling in chronic liver disease: new targets for the treatment of portal hypertension? J Hepatol 2010;53:976-80.
24. Rockey DC, Shah V. Nitric oxide biology and the liver: report of an AASLD research workshop. Hepatology 2004;39:250-7.
25. Kawada N, Klein H, Decker K. Eicosanoid-mediated contractility of hepatic stellate cells. Biochem J 1992;285:367-71.
26. Thaiss WM, Sannwald L, Kloth C, Ekert K, Hepp T, Bösmüller H, Klag T, Nikolaou K, Horger M, Kaufmann S. Quantification of Hemodynamic Changes in Chronic Liver Disease: Correlation of Perfusion-CT Data with Histopathologic Staging of Fibrosis. Acad Radiol 2018. [Epub ahead of print]. doi: 10.1016/j.acra.2018.11.009.
27. Ronot M, Asselah T, Paradis V, Michoux N, Dorvillius M, Baron G, Marcellin P, Van Beers BE, Vilgrain V. Liver fibrosis in chronic hepatitis C virus infection: differentiating minimal from intermediate fibrosis with perfusion CT. Radiology 2010;256:135-42.
28. Lazo M, Selvin E, Clark JM. Brief communication: clinical implications of short-term variability in liver function test results. Ann Intern Med 2008;148:348-52.
29. Lima-Oliveira G, Salvagno GL, Lippi G, Gelati M, Montagnana M, Danese E, Picheth G, Guidi GC. Influence of a regular, standardized meal on clinical chemistry analytes. Ann Lab Med 2012;32:250-6.
30. Nord HJ. Biopsy diagnosis of cirrhosis: blind percutaneous versus guided direct vision techniques--a review. Gastrointest Endosc 1982;28:102-4.
31. Regev A, Berho M, Jeffers LJ, Milikowski C, Molina EG, Pyrsopoulos NT, Feng ZZ, Reddy KR, Schiff ER. Sampling error and intraobserver variation in liver biopsy in patients with chronic HCV infection. Am J Gastroenterol 2002;97:2614-8.
32. Poynard T, Munteanu M, Imbert-Bismut F, Charlotte F, Thabut D, Le Calvez S, Messous D, Thibault V, Benhamou Y, Moussalli J, Ratziu V. Prospective analysis of discordant results between biochemical markers and biopsy in patients with chronic hepatitis C. Clin Chem 2004;50:1344-55.
33. Afdhal NH. Biopsy or biomarkers: is there a gold standard for diagnosis of liver fibrosis? Clin Chem 2004;50:1299-300.
34. Younossi ZM, Koenig AB, Abdelatif D, Fazel Y, Henry L, Wymer M. Global epidemiology of nonalcoholic fatty liver disease: metanalytic assessment of prevalence, incidence, and outcomes. Hepatology 2016;64:73-84.
35. Angulo P, Kleiner DE, Dam-Larsen S, Adams LA, Bjornsson ES, Charatcharoenwitthaya P, Mills PR, Keach JC, Lafferty HD, Stahler A, Haflidadottir S, Bendtsen F. Liver fibrosis, but no other histologic features, is associated with long-term outcomes of patients with nonalcoholic fatty liver disease. Gastroenterology 2015;149:389-97.e10.

36. Regini F, Colagrande S, Mazzoni LN, Busoni S, Matteuzzi B, Santini P, Wyttenbach R. Assessment of Liver Perfusion by IntraVoxel Incoherent Motion (IVIM) Magnetic Resonance-Diffusion-Weighted Imaging: Correlation With Phase-Contrast Portal Venous Flow Measurements. J Comput Assist Tomogr 2015;39:365-72.
37. Wang YX. Medical imaging in pharmaceutical clinical trials: what radiologists should know. Clin Radiol 2005;60:1051-7.

Cite this article as: Li T, Che-Nordin N, Wáng YX, Rong PF, Qiu SW, Zhang SW, Zhang P, Jiang YF, Chevallier O, Zhao F, Xiao XY, Wang W. Intravoxel incoherent motion derived liver perfusion/diffusion readouts can be reliable biomarker for the detection of viral hepatitis B induced liver fibrosis. Quant Imaging Med Surg 2019;9(3):371-385. doi: 10.21037/qims.2019.02.11

Supplementary

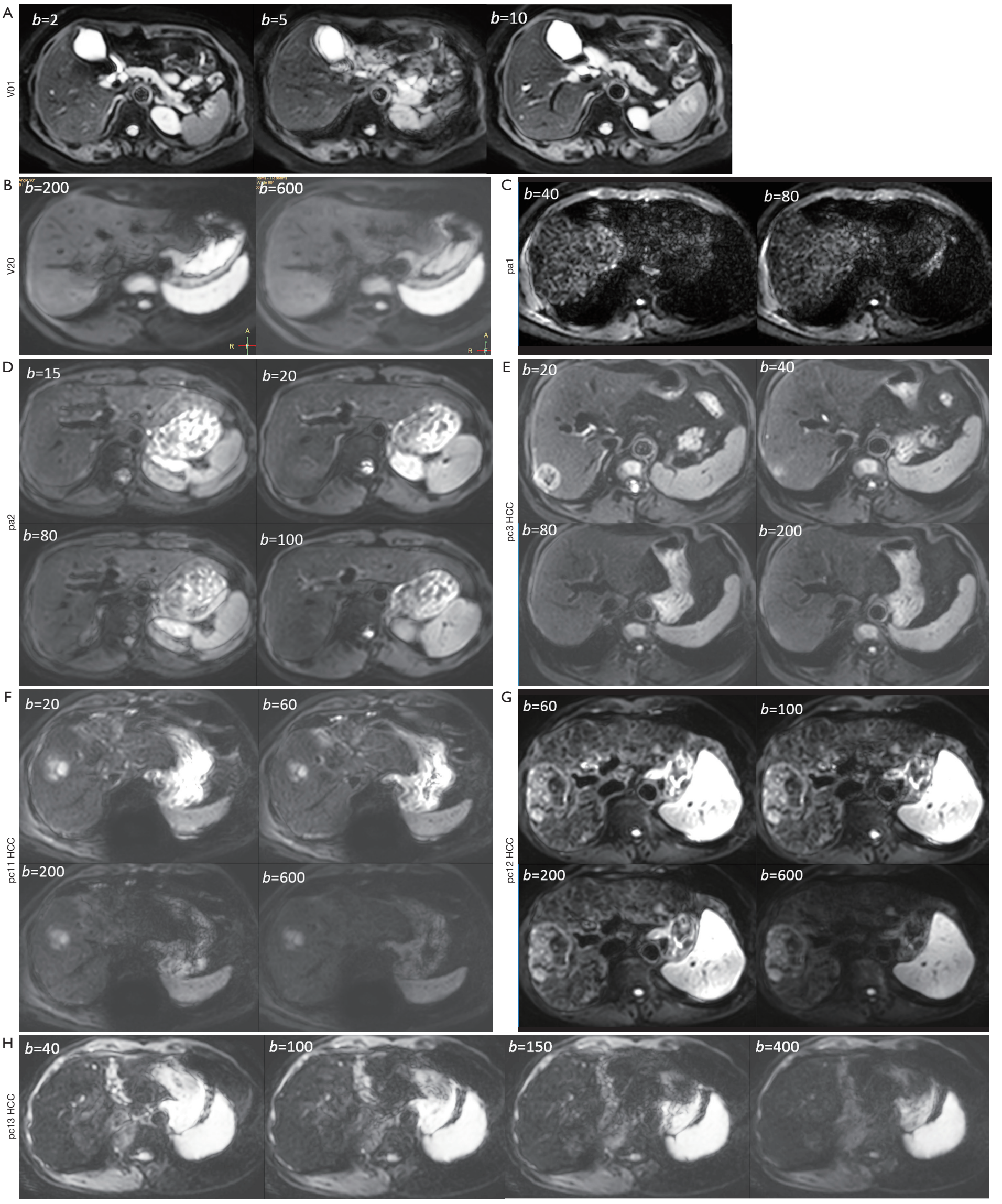

Figure S1 Example images of two volunteers (A,B) and six patients (C,D,E,F,G,H) excluded for IVIM analysis due to insufficient image quality. (A) Volunteer V01, *b* =2, 5, 10 images of the same plane. Notable position shift is present, and *b* =5 image is blurry. (B) Volunteer V20. The images of the whole set are blurry. Examples of *b* =200 and 600 images of the same plane are presented. (C) Patient pa1. The images of the whole set are blurry. Examples of *b* =40 and 80 images of the same plane are presented. (D) Patient pa2. *b* =15, 20, 80 and 100 images of the same plane are presented. *b* =15, 80 images are blurry, note the "double" portal vein appearance. Notable position shift is also present. (E) HCC patient pc3. *b* =20, 40, 80 and 200 images of the same plane are presented. Notable position shift is present. The tumor is evident on *b* =20 image, barely visible on *b* =40 image, and not visible on *b* =80 image. The portal vein appearance also differs among these four images. (F) HCC patient pc11. *b* =20, 60, 200 and 600 images of the same plane are presented. The images of the whole set are blurry and were considered un-usable for IVIM analysis. (G) HCC patient pc12. *b* =60, 100, 200 and 600 images of the same plane are presented. This case's images were considered un-usable for IVIM analysis. (H) HCC patient pc13. *b* =40, 100, 150 and 400 images of the same plane are presented. The images of the whole set are blurry and notable position shift is present. IVIM, intravoxel incoherent motion; HCC, hepatocellular carcinoma.

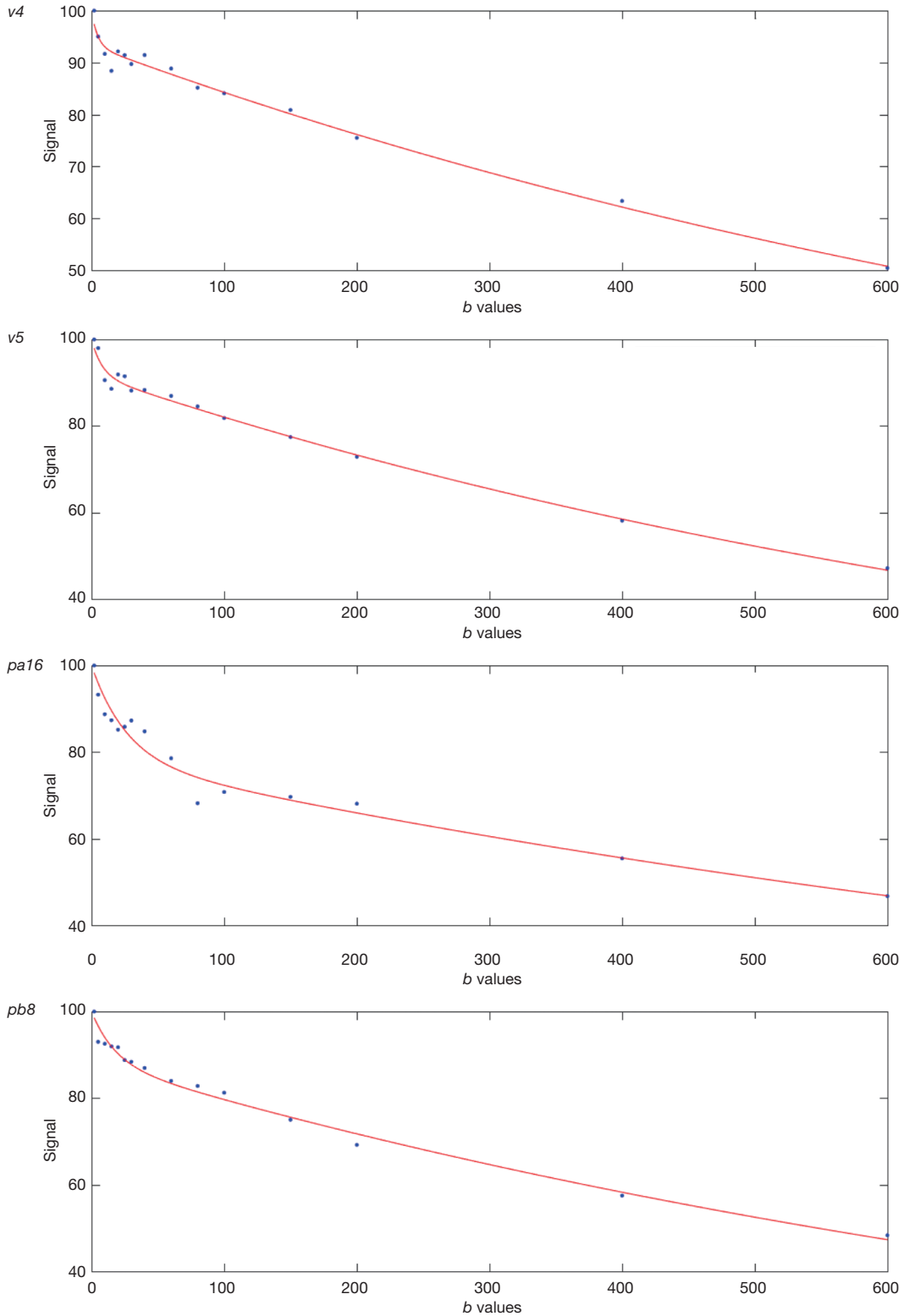

Figure S2 Poorly fitted curves of two volunteers and two patients who were excluded from final analysis.

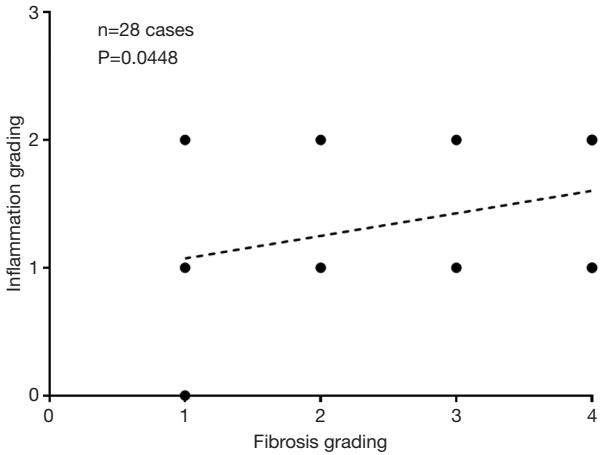

Figure S3 Correlation between fibrosis grading and inflammation. There is a weak positive correlation between fibrosis grading and inflammation grading (P=0.0448). Only liver fibrosis patients included for IVIM analysis are presented. IVIM, intravoxel incoherent motion.

Table S1 Inter-reader ROI-based measurement reproducibility data for Dfast, Dslow and PF

Patient ID	Reader 1			Reader 2		
	Dfast	Dslow	PF	Dfast	Dslow	PF
pa13	46.47	1.07	0.16	51.31	0.97	0.16
pa14	45.69	1.13	0.17	42.29	1.17	0.17
pb1	46.12	0.98	0.14	45.81	0.99	0.17
pb2	54.08	1.01	0.11	53.09	1.13	0.12
pb3	40.3	1.05	0.13	40.01	1.07	0.13
pc1	41.67	1.13	0.2	46.02	1.1	0.2
pc2	43.43	1.03	0.08	54.65	1.07	0.08
pc4	35.75	0.97	0.11	39.16	0.97	0.11
pc5	31.33	0.91	0.1	35.66	0.97	0.09
pc6	39.85	1.14	0.08	43.3	1.18	0.09
pc7	23.15	1.04	0.1	23.15	1.04	0.1
pc8	38.46	1.15	0.12	38.78	1.22	0.12
pc9	59.18	0.91	0.1	56.68	0.93	0.11
pc10	77.71	1.12	0.14	74.78	1.19	0.14

ROI, region of interest.

Table S2 Dfast, Dslow and PF values of healthy volunteers computed by seven analysis approaches (see the method section for details)

Volunteer ID	Analysis-1			Analysis-2			Analysis-3			Analysis-4			Analysis-5			Analysis-6			Analysis-7		
	Dfast	Dslow	PF	Dfast	Dslow	PF	Dfast	Dslow	PF	Dfast	Dslow	PF	Dfast	Dslow	PF	Dfast	Dslow	PF	Dfast	Dslow	PF
V02	45.333	1.194	0.167	52.96	1.231	0.154	46.964	1.209	0.164	116.686	1.2	0.227	144.001	1.233	0.216	22.685	1.194	0.112	18.789	1.159	0.089
V03	37.466	1.077	0.163	42.511	1.009	0.152	33.936	0.96	0.172	154.855	0.969	0.278	189.201	0.998	0.27	22.468	0.977	0.122	17.356	0.961	0.103
V06	37.295	1.211	0.238	40.841	1.251	0.226	32.618	1.159	0.257	73.074	1.144	0.31	80.931	1.181	0.299	28.71	1.211	0.209	20.852	1.23	0.166
V07	34.303	1.31	0.164	38.31	1.35	0.119	26.861	1.289	0.145	182.05	1.32	0.227	214.057	1.345	0.219	21.696	1.31	0.114	10.576	1.353	0.067
V08	47.877	1.232	0.141	52.648	1.251	0.135	51.957	1.251	0.135	123.37	1.232	0.221	139.904	1.251	0.215	28.548	1.232	0.106	14.34	1.29	0.078
V09	39.892	1.289	0.159	38.835	1.319	0.149	28.101	1.232	0.181	146.573	1.295	0.301	170.825	1.322	0.294	27.901	1.289	0.144	22.267	1.308	0.153
V10	49.622	1.183	0.144	53.301	1.199	0.118	56.622	1.197	0.12	206.266	1.183	0.234	230.144	1.199	0.229	30.952	1.183	0.091	16.918	1.208	0.068
V11	35.795	1.121	0.147	37.303	1.104	0.111	32.939	1.097	0.12	184.326	1.104	0.237	227.849	1.121	0.231	20.126	1.104	0.087	17.799	1.093	0.094
V12	62.388	1.094	0.149	68.68	1.112	0.143	72.915	1.138	0.139	225.078	1.103	0.274	243.852	1.119	0.27	34.926	1.094	0.107	17.988	1.097	0.079
V13	50.265	1.134	0.173	55.356	1.152	0.136	53.376	1.151	0.139	205.343	1.134	0.256	232.103	1.152	0.25	22.948	1.134	0.09	18.648	1.124	0.089
V14	51.648	1.112	0.2	56.256	1.017	0.192	53.329	1.011	0.197	239.286	0.992	0.366	263.416	1.0175	0.359	30.875	0.992	0.147	22.64	0.981	0.133
V15	39.812	1.121	0.158	39.012	1.131	0.115	31.275	1.05	0.145	80.59	1.121	0.214	85.355	1.131	0.21	21.175	1.121	0.103	18.068	1.095	0.083
V16	62.507	1.175	0.153	70.208	1.198	0.145	67.161	1.193	0.148	302.073	1.175	0.307	331.471	1.198	0.3	33.604	1.175	0.104	20.149	1.186	0.092
V17	34.698	1.017	0.181	29.479	1.028	0.177	31.896	0.914	0.219	353.835	1.017	0.394	369.992	1.028	0.392	16.399	1.017	0.127	22.687	1.025	0.156
V18	45.735	1.149	0.185	49.294	1.172	0.177	43.482	1.134	0.19	220.391	1.149	0.355	241.518	1.172	0.349	36.002	1.149	0.163	20.125	1.144	0.117
V19	35.202	1.083	0.208	39.872	1.134	0.212	33.037	1.054	0.237	72.451	1.083	0.315	85.925	1.134	0.301	21.46	1.083	0.173	9.885	1.135	0.104
V21	36.603	1.142	0.148	39.522	1.161	0.141	32.569	1.112	0.158	114.069	1.142	0.255	129.712	1.161	0.249	21.648	1.142	0.108	19.085	1.153	0.097
V22	42.35	1.318	0.159	38.605	1.435	0.154	32.845	1.378	0.171	123.211	1.418	0.278	138.046	1.435	0.273	23.597	1.418	0.125	16.177	1.338	0.113
V23	44.196	1.136	0.144	50.42	1.156	0.125	46.052	1.144	0.131	246.966	1.132	0.262	284.282	1.156	0.255	23.261	1.132	0.094	17.815	1.121	0.08
V24	55.824	1.128	0.164	58.516	1.139	0.15	56.697	1.134	0.153	195.686	1.128	0.282	206.699	1.139	0.279	36.747	1.128	0.119	27.639	1.117	0.107
Mean	44.441	1.161	0.167	47.596	1.177	0.152	43.231	1.14	0.166	178.309	1.152	0.28	200.464	1.175	0.273	26.287	1.154	0.122	18.49	1.156	0.103
SD	8.798	0.079	0.025	10.897	0.108	0.031	13.603	0.11	0.0379	75.305	0.107	0.051	79.715	0.107	0.051	5.944	0.106	0.031	4.031	0.108	0.029
CoV	0.198	0.068	0.148	0.229	0.093	0.207	0.315	0.096	0.228	0.422	0.093	0.181	0.398	0.091	0.185	0.226	0.092	0.256	0.218	0.094	0.278

Dfast and Dslow: $\times 10^{-3}$ mm^2/s. Analysis 1: segmented fitting, *Shb* =60 s/mm^2, starting from *b* =2 s/mm^2; Analysis-2: segmented fitting, with *Shb* =40 s/mm^2 and starting from *b* =2 s/mm^2; Analysis-3: full fitting, start from *b* =2 s/mm^2; Analysis-4: segmented fitting, Shb =60 s/mm^2, start from *b* =0 s/mm^2; Analysis-5: segmented fitting, *Shb* =40 s/mm^2, start from *b* =0 s/mm^2; Analysis-6: segmented fitting, *Shb* =60 s/mm^2, start from *b* =5 s/mm^2; Analysis-7: segmented fitting, *Shb* =60 s/mm^2, start from *b* =10 s/mm^2.

Table S3 Dfast, Dslow and PF values of four groups of patients computed by analysis approach-1, starting from b =2 s/mm^2 and the threshold b value was 60 s/mm^2

Patient ID	Fibrosis	Dfast (×10^{-3} mm^2/s)	Dslow (×10^{-3} mm^2/s)	PF
Group-1				
pa4	Biopsy F0	52.326	1.13	0.15
pa13	Biopsy F0	46.465	1.07	0.164
pa14	Biopsy F0	45.689	1.125	0.172
pb9	Biopsy F0	47.775	1.137	0.146
Mean	–	48.063	1.115	0.158
SD	–	2.969	0.031	0.012
Group-2				
pa5	Stage-1	38.956	0.941	0.126
pa6	Stage-1	49.672	0.954	0.107
pa10	Stage-1	43.406	0.931	0.136
pa11	Stage-1	44.999	0.931	0.11
pa12	Stage-1	55.494	1.105	0.098
pa15	Stage-1	54.538	1.02	0.085
pa18	Stage-1	43.301	0.993	0.136
pa19	Stage-1	49.303	1.043	0.136
pa20	Stage-1	84.362	1.084	0.11
pb2	Stage-1	54.084	1.012	0.114
pb8	Stage-1	37.383	1.023	0.132
Mean	–	50.500	1.003	0.117
SD	–	12.809	0.06	0.017
Group-3				
pa7	Stage-2	45.3	0.926	0.114
pa8	Stage-2	44.875	0.918	0.07
pa17	Stage-2	47.924	0.945	0.126
pb1	Stage-2	46.123	0.982	0.14
pb3	Stage-2	40.295	1.054	0.127
pb4	Stage-2	54.151	1.104	0.127
pc1	Stage-2	47.46	1.014	0.199
pb5	Stage-2	57.349	1.12	0.138
pc2	Stage-2	43.432	1.026	0.084
pc10	Stage-2	77.711	1.12	0.136
Mean	–	50.462	1.021	0.126
SD	–	10.793	0.078	0.035
Group-4				
pc4	Stage-3	35.752	0.974	0.106
pb6	Stage-3	38.458	1.146	0.117
pb7	Stage-4	35.279	0.749	0.138
pc5	Stage-4	31.326	0.91	0.103
pc6	Stage-4	39.847	1.144	0.079
pc7	Stage-4	22.042	1.037	0.095
pc9	Stage-4	59.178	0.911	0.097
Mean	–	37.412	0.982	0.105
SD	–	11.265	0.142	0.019

IVIM analysis starting from b =2 s/mm^2 and the threshold b value was 60 s/mm^2. Dfast and Dslow: ×10^{-3} mm^2/s. IVIM, intravoxel incoherent motion; ROI, region of interest.

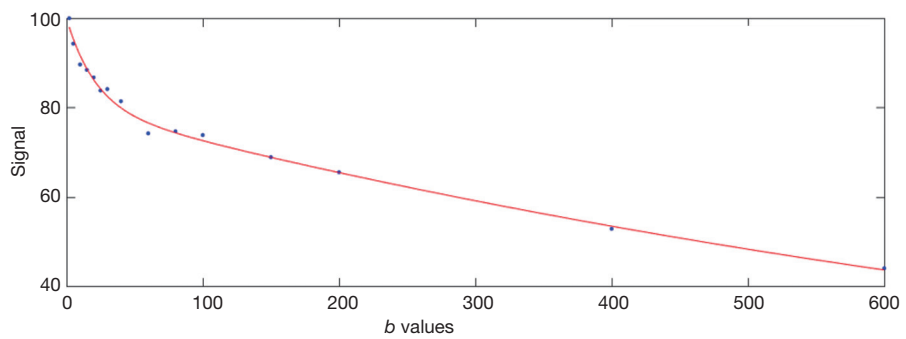

Figure S4 The acceptable fitting curve of patient-C1 with IVIM analysis starting from b =2 s/mm^2 and threshold b value of 60 s/mm^2. IVIM, intravoxel incoherent motion.